frontiers | Frontiers in Astronomy and Space Sciences

TYPE Original Research
PUBLISHED 14 January 2025
DOI 10.3389/fspas.2024.1516222

OPEN ACCESS

EDITED BY
Mirko Piersanti,
University of L'Aquila, Italy

REVIEWED BY
Yun Gong,
Wuhan University, China
Giulia D'Angelo,
Institute for Space Astrophysics and Planetology (INAF), Italy

*CORRESPONDENCE
Tao Yuan,
titus.yuan@usu.edu

RECEIVED 24 October 2024
ACCEPTED 26 December 2024
PUBLISHED 14 January 2025

CITATION
Yuan T, Pautet PD and Taylor MJ (2025) Midlatitude mesosphere and lower thermosphere variations during the extreme gannon geomagnetic storm in May 2024. *Front. Astron. Space Sci.* 11:1516222. doi: 10.3389/fspas.2024.1516222

Midlatitude mesosphere and lower thermosphere variations during the extreme gannon geomagnetic storm in May 2024

Tao Yuan[1,2]*, P. D. Pautet[1,2] and M. J. Taylor[1,2]

[1]Center for Atmosphere and Space Sciences, Utah State University, Logan, United States, [2]Physics Department, Utah State University, Logan, United States

Recent studies based upon both observations and numerical simulations have indicated the impacts of the intense geomagnetic storms induced by Coronal Mass Ejections (CMEs) on the neutral dynamics in the mesosphere and lower thermosphere (MLT). Even in the midlatitude MLT, far equatorward of subauroral zone, significant variations were reported. Aurora is one of the major dynamic drivers in the MLT in high latitudes, but observations of the neutral dynamic variations under the aurora in the storm time MLT are sparse. The lack of such MLT observations during the presence of aurora leads to a critical gap in the understanding of upper atmospheric dynamics. In this paper, we present the unprecedented observations under the aurora during the Gannon Geomagnetic Storm in May 2024 by the Na Doppler lidar at Utah State University (42°N, 112°W) and the Advanced Mesospheric Temperature mapper (AMTM) at the nearby Bear Lake observatory (BLO). Significant warming (as much as ~50 K) accompanied by fast equatorward flow in the lower thermosphere (up to ~100 m/s changes in the meridional wind above 100 km altitude) were observed. The temperature enhancement (~10 K) of the hydroxyl layer during the same period is also captured by the AMTM. Intriguingly, significant storm time depletion of sodium (Na) abundance on the topside of the mesospheric Na layer above 105 km, as much as more than 80%, was also observed. These observations provide insight for future investigations on the MLT responses to the intense geomagnetic storms, especially the role of aurora in these events.

KEYWORDS

geomagenetic storm, mesosphere and lower thermosphere (MLT), sodium layer, temperature and wind velocity fluctuations, Na lidar and AMTM

1 Introduction

Geomagnetic storm injects tremendous amount of energy and momentum into the upper thermosphere through energetic particle precipitation in the vicinity of the aurora zone, along with the considerable enhancement and fluctuations of the global electric field (Nishida et al., 1966; Banks, 1977; Pedatella and Forbes, 2011; Fejer et al., 2017). The resulting increase of Joule heating and ion drag changes the neutral temperature and composition at high latitudes dramatically, leading to large pressure gradient between the polar and equatorial regions (Fuller-Rowell et al., 1994). Such storm time meridional pressure gradient quickly generates equatorward flow in the thermosphere and expands the impacts of the geomagnetic storm globally through horizontal and vertical advection

(Burns et al., 1995). On the other hand, the zonal wind change during the storm is believed to be controlled by both the longitudinal pressure gradient and Coriolis force (Li et al., 2019). These changes become especially vigorous at high latitudes and inside the auroral oval during the intense geomagnetic storms (Kp > 8) induced by the strong Coronal Mass Ejections (CMEs) events. The strong Joule Heating of aurora induces both polarward and equatorward flow due to relatively high *in situ* pressure inside and outside the aurora (Li et al., 2023).

Recent observations have shown significant impacts of strong geomagnetic storm on the neutral dynamics in the mesosphere and lower thermosphere (MLT), even in the region equatorward of sub-auroral zone where the aurora was absent (Yuan et al., 2015; Liu et al., 2018; Yi et al., 2017; Wang et al., 2021; Ma et al., 2021; Yamazaki et al., 2024). Studying Na lidar data at middle latitudes, Yuan et al. (2015) revealed significant nightly averaged temperature enhancement in the midlatitude lower thermosphere during CME-induced intense geomagnetic storms, when the $[O]/[N_2]$ ratio in the thermosphere decreased (Zhang et al., 2014). Such storm-time temperature enhancement was further confirmed by TIMED/SABER observations from low to high latitudes (Liu et al., 2018; Wang et al., 2021). Li et al. (2018), Li et al. (2019), and Li et al. (2023) conducted several numerical simulations on the variations of mesosphere and thermosphere neutral dynamics during strong geomagnetic storms from subtropical region to polar region, utilizing Thermosphere-Ionosphere-Electrodynamics General Circulation Model (TIME-GCM). The model simulations revealed that, instead of heating, a relatively short period of cooling in the MLT during the initial phase of the storm occurs, followed by overall temperature increases. These first-principle numerical diagnosis investigations highlighted that the storm time vertical wind change is potentially the major underlying driver that generates the storm-time winds and temperature variations in the MLT. They identified three potential major sources for temperature variations in the MLT: vertical heat advection, adiabatic heating/cooling and aurora heating in the aurora zone. The first two drivers are directly associated with the vertical flow and especially important in the middle latitudes outside of the aurora zone, while the contributions to the MLT neutral dynamics directly from aurora become comparable as in the high latitudes auroral oval. The model also predicts strong equatorward meridional flow in the lower thermosphere during the geomagnetic storm, which makes the horizontal heat advection become an important source of temperature enhancement in the polar region. Overall, these major drivers all contribute to the MLT thermal budget considerably, although the contribution from an individual driver can dominate at different MLT altitude region during different storms.

However, there is still a lack of storm time simultaneous temperature and winds observations in the MLT. Although the Na Doppler lidar has the capability for such endeavor (Krueger et al., 2015), it is difficult to establish a robust storm time neutral dynamic tendency based on the limited storm time observations (Yuan et al., 2015). Except the temperature enhancement in the lower thermosphere, other features in the model results, such as the equatorward flow and the initial cooling in the MLT, have not been observed consistently. In addition, the mesosphere sodium (Na) layer, which is sensitive to the atmospheric neutral dynamic and ion-molecular chemical variations in the lower thermosphere and ionosphere E region (Cai et al., 2017; 2019), have rarely been reported to experience any consistent storm time changes. The extremely intense storm on May 10th – 11th 2024, the strongest geomagnetic storm in more than 2 decades with Kp > 9 and with Dst index going below −400 nT during its peak, provided an unprecedented opportunity to explore the MLT storm time variations. The Na Doppler lidar at Utah State University (USU) Logan campus (41.7°N, 111.8°W in geographic coordinate) was operating during this time frame, conducting nighttime observations of temperature, horizontal wind and Na number density simultaneously. Meanwhile, the USU Advanced Mesospheric Temperature Mapper, operating at nearby the Bear Lake Observatory (BLO), measured temperature variations within the hydroxyl (OH) layer in the upper mesosphere near 87 km altitude continuously. The observations during the peak of the storm on the night of DOY132 (Day Of Year 132) are especially unique and valuable, because the aurora was visible above the USU campus. These experimental data can further advance our understanding of the geomagnetic impacts on the MLT. In this paper, we report these new experimental observations in section 2, followed by the discussion based on these preliminary results in section 3. Summary of this lidar campaign is presented in section 4.

2 Storm time observations

The May 2024 Storm peaked on the late afternoon of DOY131 (10 May 2024) and the night of DOY132 (11 May 2024). The USU Na lidar conducted a campaign between DOY131 and DOY139, focusing on studying the nighttime MLT dynamics. Each night, the lidar was operating mostly between ~03:00UT and 09:00UT, during approximately the same tidal phase. The onset of the storm was around 18:00UT on DOY131, indicating the lidar observations on the night of DOY131 represent the quiet time condition, while those of DOY132 reflect the MLT variations during the early phase of the storm. In addition, during this lidar campaign, aurora was observed above the USU lidar station throughout this night (DOY132). Even though the planetary Kp > 6 during the following night (DOY133), showing the storm was still quite active, aurora was absent at the location of the lidar station. Furthermore, this campaign also marks the first time this midlatitude Na Doppler lidar has simultaneous temperature and horizontal winds observations under aurora. There were a couple of data gaps in DOY135-136 and DOY138 due to poor weather condition, however. The lidar was operating on the night of DOY125 as well. Based on the geomagnetic indexes, the data that night can also serve as a reference of quiet time MLT conditions and, thus, are included in this investigation. The lidar data during this campaign are processed with hourly temporal resolution, and smoothed vertically with a 2 km Full Width Half Max (FWHM) Gaussian window. The nightly average values of temperature and horizontal winds are calculated and investigated in this study.

2.1 The temperature and wind observations

Figure 1 shows the nightly averaged temperature (plot (a) and (c) in the left column) and meridional wind (plot (b) and (d) in the right

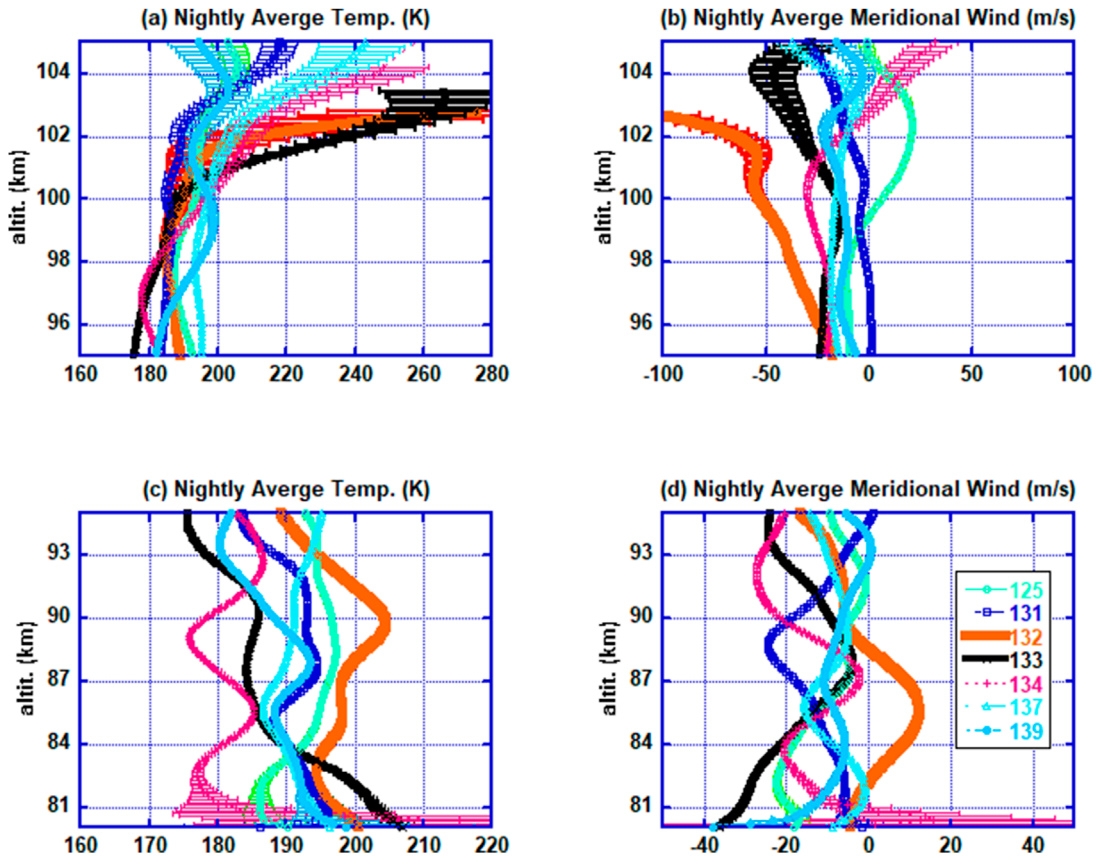

FIGURE 1
The nightly average temperature and meridional wind profiles measured by the USU Na Doppler lidar during the Extreme Gannon Geomagnetic Storm in May 2024. Plot **(A)** shows temperature profiles between 95 km and 105 km and plot **(C)** shows the profiles in altitude range of 80–95 km. Plot **(B)** and **(D)** are the same, except for meridional wind.

column) profiles in two different sections of the MLT: 80 km–95 km (plot (c) and (d)) and 95 km–105 km (plot (a) and (b)). The two sections are chosen based on the previous studies (Yuan et al., 2015), in which the lidar results demonstrated the most prominent storm time temperature variations mostly occurring above ~95 km, while the changes became insignificant below this altitude. As expected, the lidar temperature profiles demonstrate considerable warming above ~100 km altitude on the night of DOY132 and DOY133. For example, at ~ 103 km in Figure 1A, the nightly average temperature was ~280 K and 265 K on DOY132 and DOY133, respectively, while it varied between 190 K and 220 K for the geomagnetic quiet nights. As mentioned earlier, it is worth pointing out that, on the night of DOY133, no aurora was observed above the USU lidar station. Thus, the mechanism induced such warming on the night of DOY132 and DOY133 may be quite different, e.g., Joule Heating is not likely be a factor in the enhancing temperature on the night of DOY133 (see Section 3). Figure 1A also shows that the positive temperature gradient in the lower thermosphere was largest on the night of DOY132. Between ~95 km and 100 km, the storm time temperature changes are insignificant and within the standard deviation (see Figure 1C).

However, compared to the other nightly average temperatures in the upper mesosphere, there was also a noticeable temperature increase about 10 K around 90 km altitude on the night of DOY132 (see Figure 1C), the same night when significant storm time warming was observed above 100 km altitude. This temperature enhancement in the upper mesosphere is detected by the observations of the Advanced Mesospheric Temperature Mapper (AMTM) nearby at Bear Lake Observatory (BLO) as well, which measures the 2-D temperature map of the hydroxyl layer ~87 km (Pautet et al., 2014). Figure 2 illustrates the variations of the nightly average temperature of the hydroxyl layer observed by the AMTM, along with the lidar observed nightly temperatures at 87 km, where the peak of the hydroxyl layer is approximately located. The AMTM observations also present the temperature standard deviation for each night, which show no obvious correlation with the variation of geomagnetic activity. Note that there have not been geomagnetic storms related OH temperature variations reported. Therefore, it is possible this abnormal temperature increase of hydroxyl layer is related to this super storm. On the other hand, such potential connection could be complicated by the other active neutral dynamic processes. Based on the AMTM observations in Figure 2, the temperature variations show a quasi-6-day wave signature. The quasi-6-day wave, a westward propagating wavenumber 1 planetary wave, is one of the most prominent planetary waves (Forbes and Zhang, 2017). Coincidently, its temperature and wind modulations

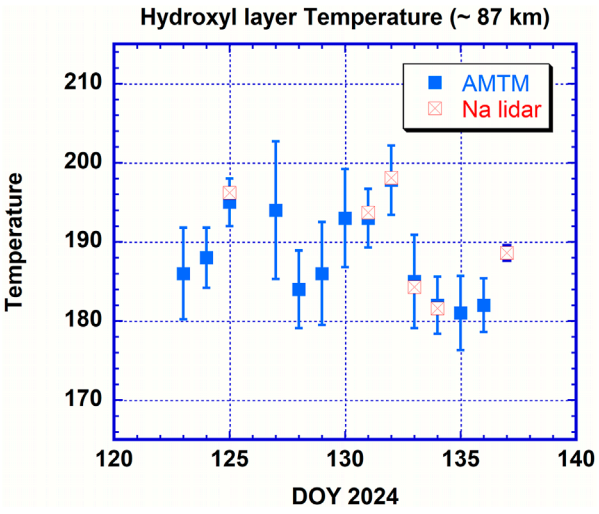

FIGURE 2
The nightly average temperatures near 87 km measured by AMTM (blue squares), along with the standard deviation of the temperature each night. The USU Na lidar measured nightly average temperatures at 87 km (squares with cross inside) are also illustrated in the plot.

have been reported to peak in May and September in the mesosphere (Talaat et al., 2001, Liu et al., 2004; Qin et al., 2019). Thus, this temperature anomaly could also be induced by a quasi-6-day wave, peaking coincidently with the Gannon super storm. Overall, the relation between this observed storm time warming in the hydroxyl layer and the geomagnetic activities needs further investigations.

As far as the horizontal wind variations, previous investigations have not been able to establish consistent storm time horizontal wind tendency, likely due to the highly variable nature of the horizontal wind in the lower thermosphere, even during the quiet time (Yuan et al., 2024). Figures 1B,D illustrate the nightly average meridional wind profiles during this lidar campaign. Figure 1B shows the meridional wind during the night of DOY132 changed to equatorward flow in the lower thermosphere above ~95 km. Near 102.5 km, the meridional wind increased to ~100 m/s toward the equator. In the lower altitudes (Figure 1D), however, the meridional wind turned slightly northward (polarward), peaking at ~ 12 m/s, near 86 km altitude, also noticeably larger compared to those of the other nights and is coincided with the AMTM observed hydroxyl temperature enhancement. The meridional wind quickly recovered the following day (DOY133) to its pre-storm feature, even though the Kp value was still high. It is worth pointing out that such equatorward acceleration during the peak of the storm in the midlatitude lower thermosphere was indeed observed by sounding rockets during some previous CME induced storms (Smith, 1968; Haerendel, 1972; Rishbeth et al., 1972; Fagundes et al., 1995). On the other hand, such storm time meridional wind pattern in the MLT is found to be inconsistent in the previous lidar storm time observations. In addition, the lidar observed zonal wind variations during the same time (not shown) do not show any consistent tendency at all.

Figure 3 shows the nightly average temperature (Figure 3A) and wind (Figure 3B) variations at 102 km altitude during this lidar campaign, along with the Dst index. Although the temperature on DOY132 (larger than 210 K) is about 20 K warmer than that of the pre-storm (~190 K on DOY131), the warmest temperature at this altitude was observed on the second day of the storm (DOY133), close to 240 K. As the storm settled on DOY134, the temperature dropped to slightly below 210 K. The nightly average temperature kept dropping back to the pre-storm level, ~205 K on DOY137 and ~195 K on DOY139, respectively. In addition, the Na lidar observed increasing variability of the temperature and the meridional wind were observed during this super storm in the lower thermosphere. Figures 3C, D illustrates the variance of the temperature and meridional wind during each night in the lower thermosphere at 101 km (purple dot line), 100.5 km (blue dash line), 100 km (green dash-dot line), 99.5 km (yellow dash-dot-dot-dot line) and 99 km (red long dashes line), calculated based on the hourly average lidar data. The largest temperature variance in the lower thermosphere was seen during the night of DOY133, the second night of the storm, even though the variance started to increase on DOY132. For meridional wind, on the other hand, the large variabilities were observed on the night of both DOY132, DOY133. On the night of DOY134, the meridional wind variance was still considerably larger than that of the pre-storm, but became much less than the storm time variance.

2.2 Mesospheric Na layer observations

The mesospheric Na layer, located between ~75 km and 110 km altitude, is formed by the combination of meteor ablations and the unique chemical reaction processes in the MLT that are sensitive to the neutral dynamic conditions, such as temperature and winds (Plane et al., 2015). In the nighttime lower thermosphere, the lifetime of atomic Na is fairly long due to slow chemical reaction rates under geomagnetic quiet time conditions, making its variation dominated by atmospheric neutral dynamics processes, such as tides and gravity waves (Cai et al., 2017; Cai et al., 2019). During severe geomagnetic storm, however, when increasing energetic particle precipitation and electric field occur in the thermosphere-ionosphere system, the Na layer, especially the topside of the layer, is expected to have some considerable variations. This is because the Na production in the lower thermosphere heavily relies on ion chemistry, which is slightly anti-correlated to the neutral temperature (Plane 2003). Yet, there is little experimental evidence to support this hypothesis.

Figure 4 demonstrates the variations of some key parameters of the mesospheric Na layer vs the changing Dst index during this lidar campaign. As the figure shows, the nightly average Na abundance between 105 km and 115 km (Figure 4A) dropped abruptly when the storm arrived on the night of DOY132: the nightly averaged value decreased from ~3.8 × 10^7/m^2 the night before (DOY131) to ~6.4 × 10^6/m^2, a more than 80% decrease. On the night of DOY133 when the storm was still active, the nightly average Na abundance above 105 km was still very low, ~9.8×10^6/m^2, and close to that of DOY132. Such Na depletion results in that the lidar temperature and wind measurements could not reach ~105 km on the nights of DOY132 and DOY133 (Figure 1) as they did during the other nights (the lidar data with measurement uncertainties larger than 20 K are treated as bad data and excluded in this study). The Na abundance

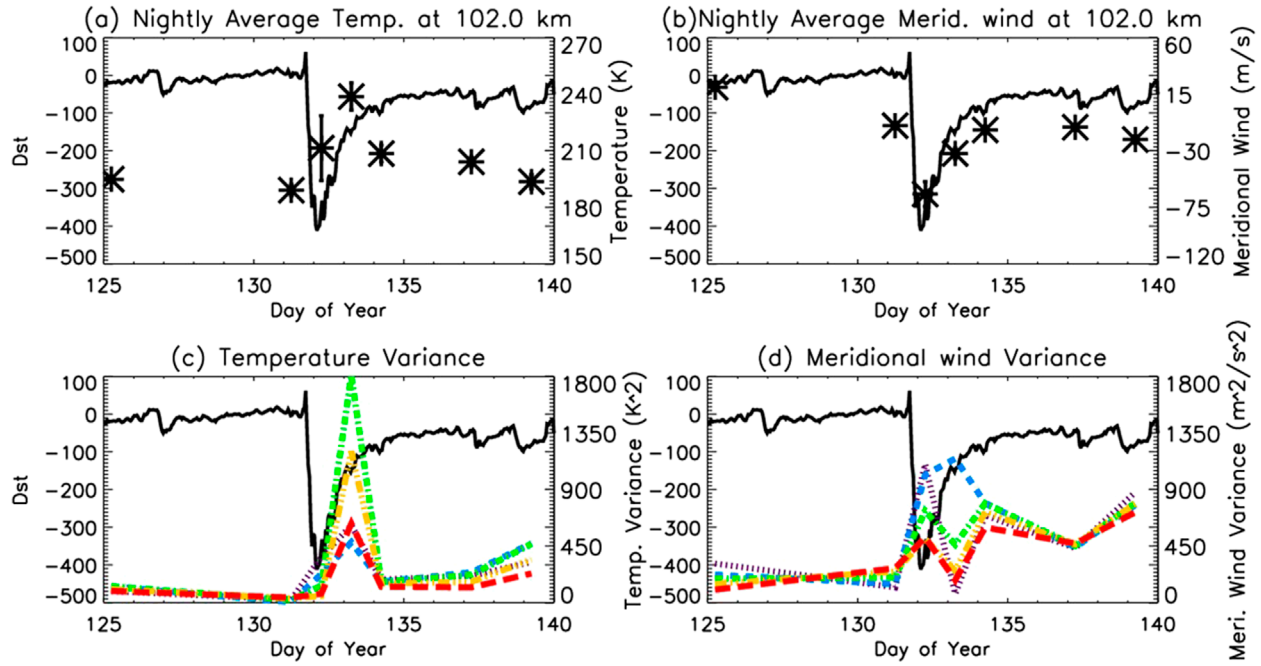

FIGURE 3
The lidar measured variations of the nightly average temperature **(A)** and meridional wind **(B)** at 102 km, along with the temperature variance **(C)** and meridional wind **(D)** variance at 99 km (red long dashes line), 99.5 km (yellow dash-dot-dot-dot line), 100 km (green dash-dot line), 100.5 km (blue dash line) and 101 km (purple dot line).

on the top side went back to the pre-storm level on DOY134, ~2.7 × $10^7/m^2$, similar to that of DOY125 (1.9 × $10^7/m^2$). Note that the topside Na abundance dropped again on the night of DOY139, down to ~1.4 × $10^7/m^2$, which was coincided with a weaker storm with its lowest Dst ~100 nT. The Na abundance between 85 km and 95 km altitude (Figure 4B), on the other hand, does not demonstrate any considerable variations that are associated with the Dst index. Looking at the altitude on the topside of the layer where the nightly average Na number density equals to $10^7/m^3$ (Figure 4C), it dropped about 6 km from ~111 km altitude on the night of DOY131 to near 105 km on DOY132 and DOY133. Similar to the aforementioned variation of the topside Na abundance throughout the storm, this altitude recovered to ~112 km on DOY134 and 110 on DOY137, but dropped again down to ~107 km during the weaker storm on the night of DOY139. On the other hand, the variations of peak altitude of the mesospheric Na layer (Figure 4D), where the maximum Na number density occurs, does not show any noticeable correlation with the Dst index. Overall, this super intense geomagnetic storm caused significant Na depletion on the topside of the Na layer.

To see the potential relation between Na number density variation and the geomagnetic activity below 105 km, utilizing the hourly Na lidar data during this campaign, the correlation coefficient between the Na number density and Dst index at each altitude between 80 km and 105 km altitude is calculated and shown in Figure 5. Between 80 km and 98 km altitude, the correlation coefficient varies from ~ - 0.2 to 0.2, implicating no correlation between the Na number density and the geomagnetic index. Above 98 km, however, it increases quickly from 0.2 to larger than 0.6 at 105 km, which indicates positive correlation between the two variables above 100 km. It worth pointing out that the hourly Na number density data also contain atmospheric gravity wave modulations and variations, in addition to the geomagnetic variation, which makes this correlation relation more complex. Indeed, Yuan et al. (2024) found gravity wave behavior contribute considerably to the large variability in static state lower thermosphere. But overall, the hourly Na density still show reasonably strong positive correlation to the Dst index above ~98 km, demonstrating unprecedented changes in the mesospheric Na layer, below 105 km altitude, during the Gannon Geomagnetic Super Storm.

3 Discussion

As described in section 2, during the Gannon Geomagnetic Super Storm, in the midlatitude lower thermosphere, the Na Doppler lidar at USU observed considerable temperature enhancement by several tens of Kelvin (Figure 1A) and equatorward flow acceleration and speed (~100 m/s) in the meridional wind (Figure 1B) right above 100 km altitude. Yuan et al. (2015) first reported temperature enhancement in the midlatitude lower thermosphere during several CME induced strong geomagnetic storms (Kp > 8), while there has no report on the storm-time horizontal wind changes in the MLT. Several first principle numerical simulations, utilizing TIME-GCM (Li et al., 2018; Li et al., 2019; Li et al., 2023), have been conducted to investigate and understand the potential underlying mechanisms of these MLT variations during the intense geomagnetic storms (Kp > 8). Although the magnitude of the variations in these simulations is small compared to the lidar observations (Yuan et al., 2015), these numerical studies are able to reproduce the storm time temperature enhancement,

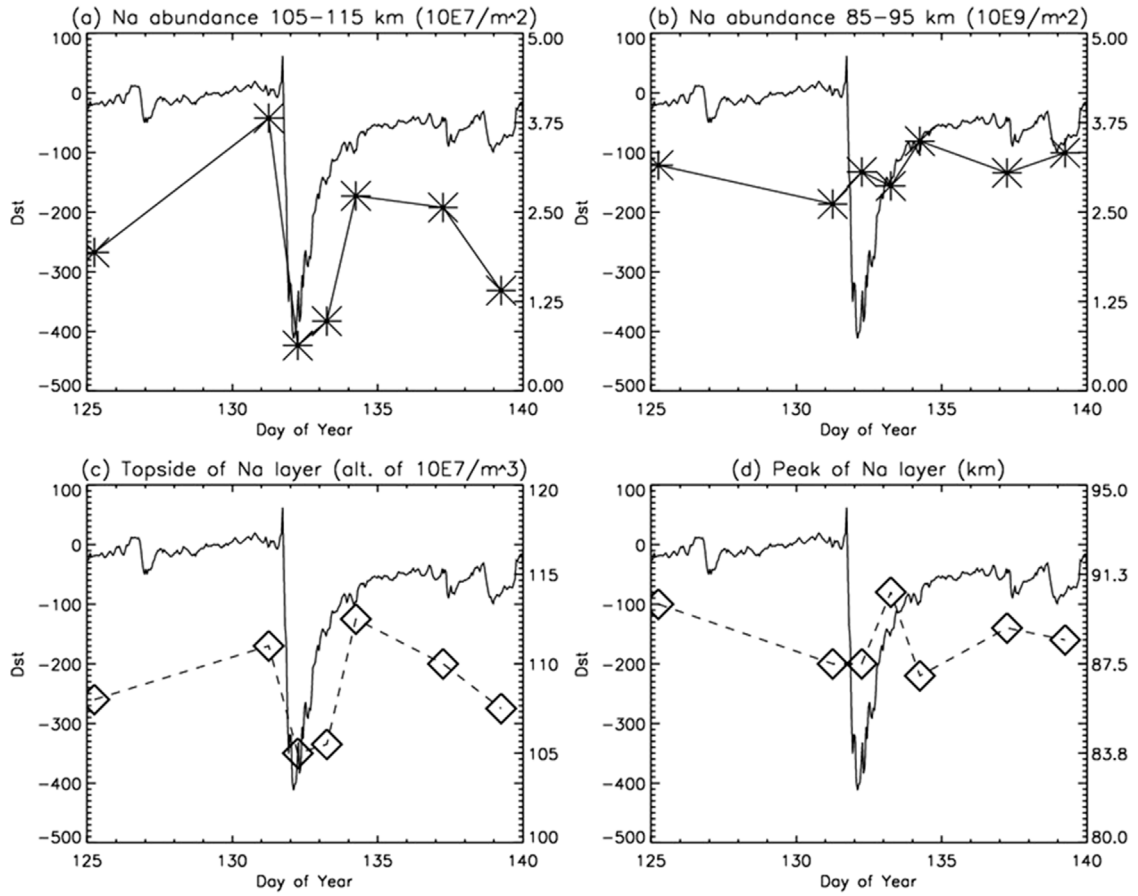

FIGURE 4
The mesospheric Na layer variation during the Extreme Gannon Geomagnetic Storm: The nightly average Na abundance between 105 km and 115 km (asterisk) **(A)** and those between 85 km and 95 km (asterisk) **(B)**; the altitude of the nightly average Na number density of $10E^{07}/m^3$ (diamond) **(C)**, the peak altitude of the mesospheric Na layer (diamond) **(D)**.

along with the equatorward acceleration of the meridional wind in the lower thermosphere in the MLT equatorward of the subauroral zone. Based on the diagnosis studies of the model outputs, the CME event deposits tremendous amount of energy in the thermosphere and causes enhanced Joule heating and upwelling motion inside the polar cap. The associated geomagnetic storm then induces large pressure gradient between the high latitude and the equatorial thermosphere throughout the storm, leading to an equatorward and downward flow in the subauroral zone and midlatitude, where the aurora is absent. The middle latitudes lower thermosphere can be indeed affected by this flow as well during strong geomagnetic storms. Thus, the downward flow increases the vertical wind in the thermosphere, leading to the enhanced vertical heat advection and adiabatic heating in the lower thermosphere. The aurora heating (Joule Heating) becomes an important heating source in the high latitude lower thermosphere (Li et al., 2023), but is not expected to contribute significantly to the MLT region outside the aurora oval. In addition, a short period of upward flow and adiabatic cooling are predicted in these simulations in the lower thermosphere during the initial phase of the storm. This is believed to be part of the upwelling movement of the upper atmosphere during this phase of the storm. Although considerable temperature enhancement and the equatorward flow in the lower thermosphere were indeed observed during the May 2024 super storm, distinct to the previous storm time lidar observations (Yuan et al., 2015), the aurora appeared at the USU lidar station on the night of DOY132. This implicates that these lidar observed dynamic changes above ~100 km on this night could also be significantly contributed by the Joule Heating associated with the aurora, while the warm temperature on the night of DOY133 in the same region may be mainly related to the storm time adiabatic heating and/or vertical heat advection due to the storm time enhanced downward flow, as suggested by the above numerical investigations.

The lidar observed considerable depletion of Na abundance on the topside of the mesospheric Na layer on the nights of DOY132 and DOY133, on the other hand, was not observed in previous storm time lidar campaigns. And, to our knowledge, there has been no theoretical investigations on geomagnetic storm's potential impact on the mesospheric metal layers, even though the molecular ions, which are critical for these metallic atoms variabilities in the E region ionosphere, experience drastic changes during geomagnetic storm (Banks et al., 1974; Strickland et al., 1976; Mertens et al., 2009). Nonetheless, it is possible that the aforementioned enhanced downward flow during the intense geomagnetic storm can transfer the Na atoms downward (dynamic transfer mechanism), leading

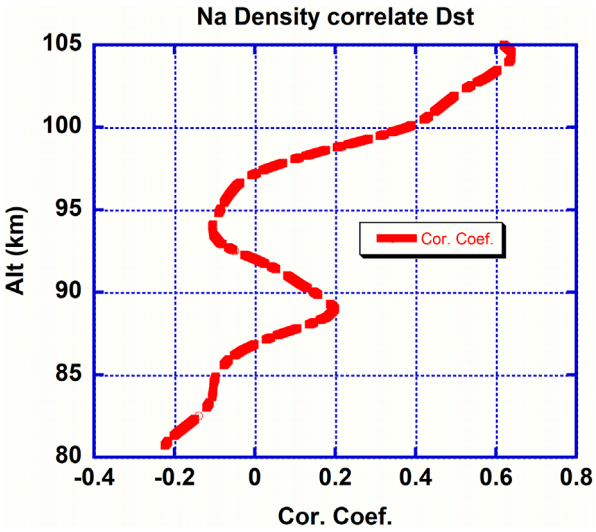

FIGURE 5
The correlation coefficient profile of Na number density vs Dst index, based on the hourly Na number density profiles by the USU Na lidar and Dst index during the Extreme Gannon Geomagnetic Storm in May 2024.

to decreasing Na number density in the lower thermosphere. The fact that this Na depletion was also observed on both the night of DOY133 and DOY132 suggests this is indeed a plausible mechanism. From the chemistry perspective, the Na chemical production in the lower thermosphere is slightly anti-correlated with the temperature as well (Plane, 2003; Plane et al., 2015). This could also relate the observed topside Na depletion with the considerable storm time temperature enhancement on the night of DOY132 and DOY133. In addition, one of the major reactions in the aforementioned Na chemical production mechanism is the increasing Na ionization through the atomic Na reactions with NO^+ and O_2^+ in the E region. Due to the strong particle participation during the occurrence of aurora, the storm time large variations of molecular ions, such as NO^+ and O_2^+, that are essential for the ionization of Na atoms, could certainly disturb the Na density on the topside of the mesospheric metal layers, leading to the production of more Na^+ while less neutral Na atoms. This potential ion-chemical mechanism, along with the aforementioned dynamic transfer mechanism, could lead to the depletion of many the neutral metal species in the lower thermosphere as well, such as Fe, Ca, etc., during the extreme geomagnetic storms of this level when the downward flow is strong. Observations from the other types of fluorescence lidar during intense geomagnetic storms, especially with the appearance of aurora, would be needed to validate this hypothesis. Chu et al. (2020) reported E region column abundance of Fe and Na variations corresponding to the aurora activities at McMurdo station (77.84°S, 166.67°E) during quiet time. This study reported the Fe abundance corresponded well with aurora and ionization, but not for the Na abundance. This implicates the USU lidar observed storm time depletion of Na on the topside of the Na layer may be more likely to be induced by the MLT neutral dynamic variations, such as winds (the aforementioned dynamic transfer mechanism). Of course, numerical simulations of the advance chemistry models would also be required to understand this newly discovered storm time feature in the lower thermosphere.

4 Summary

The Na Doppler lidar and AMTM at Utah State University conducted a multi-day campaign during the extreme geomagnetic storm in May 2024, the strongest storm in about 2 decades. These midlatitude MLT observations show considerable temperature enhancement, as much as ~ 50 K near and above 102 km, in the lower thermosphere on the nights of DOY132 (May 11th, the first night of the storm) and DOY133. In addition to the increasing temperature, large equatorward (southward) meridional flow (~100 m/s near 102 km altitude) was also observed by the Na lidar above 100 km on the night of DOY132 when aurora appeared above the lidar station. The temperature and meridional wind of the lower thermosphere also demonstrate large variabilities during the storm. During the same night, considerable Na depletion on the top side of the mesospheric Na layer, more than 80% decrease of Na abundance above 105 km altitude, was also observed for the first time.

Recent first principle numerical studies demonstrate the geomagnetic storm impacts on the midlatitude MLT neutral dynamic equatorward of the aurora oval mainly through vertical heat advection and adiabatic processes due to the large storm time meridional pressure gradient in the thermosphere. The contribution of aurora to the storm time MLT variations is believed to be only significant at high latitudes. However, the appearance of aurora above this midlatitude lidar station during the night of DOY132 complicates the understanding of these observations. In addition to the storm time enhanced downward flow, the aurora and the associated electrodynamic processes, such as Joule Heating and increasing ionization in the lower thermosphere, could also play a major role in the lidar observed variations on the night of DOY132: the increasing temperature and the Na depletion on the top side of the metal layer. The intensive warming on the night of DOY133, on the other hand, may be most likely due to downward heat advection and adiabatic heating induced by the storm time enhanced downward flow. Therefore, although this lidar campaign provided an unprecedented opportunity to study the MLT variations in the aurora oval, more observations, especially storm time observations from the other type of fluorescence lidar, are needed to further investigate the storm time MLT variations. Coupled with these observations, the numerical studies will also be required to understand the mechanisms that drive these variations, and fully grasp the geomagnetic storm impacts on the atmosphere.

Data availability statement

Publicly available datasets were analyzed in this study. This data can be found here: The USU Na lidar data of this investigation, along with the all the USU Na lidar data, are available at 315 https://doi.org/10.15142/T33H26, which is managed by the USU library DigitalCommons [Yuan, 2018]. 316 The AMTM data used in this study is available through the Harvard Dataverse repository 317

at https://dataverse.harvard.edu/dataset.xhtml?persistentId=doi:10.7910/DVN/YEZKUU.

Author contributions

TY: Conceptualization, Data curation, Formal Analysis, Funding acquisition, Investigation, Methodology, Project administration, Supervision, Validation, Visualization, Writing–original draft, Writing–review and editing. PP: Data curation, Visualization, Writing–review and editing. MT: Funding acquisition, Resources, Data curation, Writing–review and editing.

Funding

The author(s) declare that financial support was received for the research, authorship, and/or publication of this article. The work by the USU Na lidar was supported by NNH12ZDA006O-HPEXMO: Atmospheric Wave Experiment. The USU AMTM was designed under the Air Force DURIP grant F49620-02-1-0258, and operated under the NASA contract number 80GSFC18C0007.

Conflict of interest

The authors declare that the research was conducted in the absence of any commercial or financial relationships that could be construed as a potential conflict of interest.

Generative AI statement

The authors declare that no Generative AI was used in the creation of this manuscript.

Publisher's note

References

Banks, P. M. (1977). Observations of joule and particle heating in the auroral zone. *J. Atmos. Terr. Phys.* 39 (2), 179–193. doi:10.1016/0021-9169(77)90112-X

Banks, P. M., Chappell, C. R., and Nagy, A. F. (1974). A new model for the interaction of auroral electrons with the atmosphere: spectral degradation, backscatter, optical emission, and ionization. *J. Geophys. Res.* 79 (10), 1459–1470. doi:10.1029/ja079i010p01459

Burns, A. G., Killeen, T. L., Deng, W., Carignan, G. R., and Roble, R. G. (1995). Geomagnetic storm effects in the low-to middle-latitude upper thermosphere. *J. Geophys. Res.* 100 (A8), 14673–14691. doi:10.1029/94JA03232

Cai, X., Yuan, T., Eccles, J. V., Pedatella, N. M., Xi, X., Ban, C., et al. (2019). A numerical investigation on the variation of sodium ion and observed thermospheric sodium layer at cerro pachón, Chile during equinox. *J. Geophys. Res. Space Phys.* 124, 10395–10414. doi:10.1029/2018JA025927

Cai, X., Yuan, T., and Vincent Eccles, J. (2017). A numerical simulation to investigate the mechanism of high altitude Na_s formation in the mid-latitude E region above 100 km. *J. Geophys. Res. Space Phys.* 122. doi:10.1002/2016JA023764

Chu, X., Nishimura, Y., Xu, Z., Yu, Z., Plane, J. M. C., Gardner, C. S., et al. (2020). First simultaneous lidar observations of thermosphere-ionosphere Fe and Na (TIFe and TINa) layers at McMurdo (77.84°S, 166.67°E), Antarctica with concurrent measurements of aurora activity, enhanced ionization layers, and converging electric field. *Geophys. Res. Lett.* 47, e2020GL090181. doi:10.1029/2020GL090181

Fagundes, P. R., Sahai, Y., Bittencourt, J. A., and Takahashi, H. (1995). Observations of thermospheric neutral winds and temperatures at Cachoeira Paulista (23°S, 45°W) during a geomagnetic storm. *Adv. Space Res.* 16 (5), 27–30. doi:10.1016/0273-1177(95)00169-F

Fejer, B. G., Blanc, M., and Richmond, A. D. (2017). Post-storm middle and low-latitude ionospheric electric fields effects. *Space Sci. Rev.* 206 (1–4), 407–429. doi:10.1007/s11214-016-0320-x

Forbes, J. M., and Zhang, X. (2017). The quasi-6 day wave and its interactions with solar tides. *J. Geophys. Res. Space Phys.* 122, 4764–4776. doi:10.1002/2017JA023954

Fuller-Rowell, T. J., Codrescu, M. V., Moffett, R. J., and Quegan, S. (1994). Response of the thermosphere and ionosphere to geomagnetic storms. *J. Geophys. Res.* 99 (A3), 3893–3914. doi:10.1029/93JA02015

Haerendel, G. (1972). "Electric fields and their effects in the ionosphere," in *The upper atmosphere: Part IV of solar-terrestrial physics/1970 comprising the proceedings of the international symposium on solar-terrestrial physics held in Leningrad, USSR87-116*. Editors S. A. Bowhill, and E. R. Dyer (Springer Netherlands), 87–116. doi:10.1007/978-94-010-3132-5_6

Krueger, D. A., She, C.-Y., and Yuan, T. (2015). Retrieving mesopause temperature and line-of-sight wind from full-diurnal-cycle Na lidar observations. *Appl. Opt.* 54 (32), 9469–9489. doi:10.1364/ao.54.009469

Li, J., Wang, W., Lu, J., Yuan, T., Yue, J., Liu, X., et al. (2018). On the responses of mesosphere and lower thermosphere temperatures to geomagnetic storms at low and middle latitudes. *Geophys. Res. Lett.* 45. doi:10.1029/2018GL078968

Li, J., Wang, W., Lu, J., Yue, J., Burns, A., Yuan, T., et al. (2019). A modeling study of the responses of mesosphere and lower thermosphere winds to geomagnetic storms at middle latitudes. *J. Geophys. Res. Space Phys.* 124, 3666–3680. doi:10.1029/2019JA026533

Li, J., Wei, G., Wang, W., Luo, Q., Lu, J., Tian, Y., et al. (2023). A modeling study on the responses of the mesosphere and lower thermosphere (MLT) temperature to the initial and main phases of geomagnetic storms at high latitudes. *J. Geophys. Res. Atmos.* 128, e2022JD038348. doi:10.1029/2022JD038348

Liu, H.-L., Talaat, E. R., Roble, R. G., Lieberman, R. S., Riggin, D. M., and Yee, J.-H. (2004). The 6.5-day wave and its seasonal variability in the middle and upper atmosphere. *J. Geophys. Res.* 109 (D21), D21112. doi:10.1029/2004JD004795

Liu, X., Yue, J., Wang, W., Xu, J., Zhang, Y., Li, J., et al. (2018). Responses of lower thermospheric temperature to the 2013 St. Patrick's Day geomagnetic storm. *Geophys. Res. Lett.* 45, 4656–4664. doi:10.1029/2018GL078039

Ma, Z., Gong, Y., Zhang, S., Xue, J., Luo, J., Zhou, Q., et al. (2021). Study of a quasi-27-day wave in the MLT region during recurrent geomagnetic storms in autumn 2018. *J. Geophys. Res. Space Phys.* 126, e2020JA028865. doi:10.1029/2020JA028865

Mertens, C. J., Winick, J. R., Picard, R. H., Evans, D. S., López-Puertas, M., Wintersteiner, P. P., et al. (2009). Influence of solar-geomagnetic disturbances on SABER measurements of 4.3 μm emission and the retrieval of kinetic temperature and carbon dioxide. *Adv. Space Res.* 43 (9), 1325–1336. doi:10.1016/j.asr.2008.10.029

Nishida, A., Iwasaki, N., and Nagata, T. (1966). The origin of fluctuations in the equatorial electrojet: a new type of geomagnetic variation. *Ann. Geophys.* 22, 5549–5559.

Pautet, P.-D., Talor, M. J., Pendleton, W. R., Jr., Zhao, Y., Yuan, T., Esplin, R., et al. (2014). Advanced mesospheric temperature mapper for high-latitude airglow studies. *Appl. Opt.* 53 (26), 5934–5943. doi:10.1364/ao.53.005934

Pedatella, N. M., and Forbes, J. M. (2011). Electrodynamic response of the ionosphere to high-speed solar wind streams. *J. Geophys. Res.* 116, A12310. doi:10.1029/2011JA017050

Plane, J. M. C. (2003). Atmospheric chemistry of meteoric metals. *Chem. Rev.* 103 (12), 4963–4984. doi:10.1021/cr0205309

Plane, J. M. C., Feng, W., and Dawkins, E. C. M. (2015). The mesosphere and metals: chemistry and changes. *Chem. Rev.* 115, 4497–4541. doi:10.1021/cr500501m

Qin, Y., Gu, S.-Y., Dou, X., Gong, Y., Chen, G., Zhang, S., et al. (2019). Climatology of the quasi-6-day wave in the mesopause region and its modulations on total electron content during 2003–2017. *J. Geophys. Res. Space Phys.* 124, 573–583. doi:10.1029/2018JA025981

Rishbeth, H., Rees, D., and Kaiser, T. R. (1972). Winds and temperatures in the auroral zone and their relations to geomagnetic activity: discussion. *Philos. Trans. R. Soc. A* 271 (1217), 573–575. Available at: http://www.jstor.org/stable/74114.

Smith, L. B. (1968). An observation of strong thermospheric winds during a geomagnetic storm. *J. Geophys Res.* 73 (15), 4959–4963. doi:10.1029/JA073i015p04959

Strickland, D. J., Book, D. L., Coffey, T. P., and Fedder, J. A. (1976). Transport equation techniques for the deposition of auroral electrons. *J. Geophys. Res.* 81 (16), 2755–2764. doi:10.1029/ja081i016p02755

Talaat, E. R., Yee, J.-H., and Zhu, X. (2001). Observations of the 6.5-day wave in the mesosphere and lower thermosphere. *J. Geophys. Res.* 106 (D18), 20715–20723. doi:10.1029/2001JD900227

Wang, N., Yue, J., Wang, W., Qian, L., Jian, L., and Zhang, J. (2021). A comparison of the CIR- and CME-induced geomagnetic activity effects on mesosphere and lower thermospheric temperature. *J. Geophys. Res. Space Phys.* 126, e2020JA029029. doi:10.1029/2020JA029029

Yamazaki, Y., Stolle, C., Stephan, C., and Mlynczak, M. G. (2024). Lower thermospheric temperature response to geomagnetic activity at high latitudes. *J. Geophys. Res. Space Phys.* 129, e2024JA032639. doi:10.1029/2024JA032639

Yi, W., Reid, I. M., Xue, X., Younger, J. P., Murphy, D. J., Chen, T., et al. (2017). Response of neutral mesospheric density to geomagnetic forcing. *Geophys. Res. Lett.* 44, 8647–8655. doi:10.1002/2017GL074813

Yuan, T., Pautet, P.-D., Zia, K., Zhao, Y., and Taylor, M. J. (2024). The variations of gravity wave activities during the formation of the large horizontal wind shears in the static state lower thermosphere. *Earth Space Sci.* 11, e2023EA003296. doi:10.1029/2023EA003296

Yuan, T., Zhang, Y., Cai, X., She, C.-Y., and Paxton, L. J. (2015). Impacts of CME induced geomagnetic storms on the mid-latitude mesosphere and lower thermosphere observed by a sodium lidar and TIMED/GUVI. *Geophys. Res. Lett.* 42, 7295–7302. doi:10.1002/2015GL064860

Zhang, Y., Paxton, L. J., Morrison, D., Marsh, D., and Kil, H. (2014). Storm-time behaviors of O/N2 and NO variations. *J. Atmos. Sol. Terr. Phys.* 114, 42–49. doi:10.1016/j.jastp.2014.04.003